Klein-bottle quadrupole insulators and Dirac semimetals

Chang-An Li,[1,*] Junsong Sun,[2] Song-Bo Zhang,[3] Huaiming Guo,[2] and Björn Trauzettel[1,4]
[1]*Institute for Theoretical Physics and Astrophysics, University of Würzburg, 97074 Würzburg, Germany*
[2]*School of Physics, Beihang University, Beijing 100191, China*
[3]*International Center for Quantum Design of Functional Materials, Hefei National Research Center for Physical Sciences at the Microscale, University of Science and Technology of China, Hefei, Anhui 230026, China*
[4]*Würzburg-Dresden Cluster of Excellence ct.qmat, 97074 Würzburg, Germany*

(Received 15 September 2023; accepted 28 November 2023; published 8 December 2023)

The Benalcazar-Bernevig-Hughes (BBH) quadrupole insulator model is a cornerstone model for higher-order topological phases. It requires π-flux threading through each plaquette of the two-dimensional Su-Schrieffer-Heeger model. Recent studies showed that particular π-flux patterns can modify the fundamental domain of momentum space from the shape of a torus to a Klein bottle with emerging topological phases. By designing different π-flux patterns, we propose two types of Klein-bottle BBH models. These models show rich topological phases, including Klein-bottle quadrupole insulators and Dirac semimetals. The phase with nontrivial Klein-bottle topology shows twined edge modes at open boundaries. These edge modes can further support second-order topology, yielding a quadrupole insulator. Remarkably, both models are robust against flux perturbations. Moreover, we show that different π-flux patterns dramatically affect the phase diagram of the Klein-bottle BBH models. Going beyond the original BBH model, Dirac semimetal phases emerge in Klein-bottle BBH models featured by the coexistence of twined edge modes and bulk Dirac points.

DOI: 10.1103/PhysRevB.108.235412

I. INTRODUCTION

The quadrupole insulator model proposed by Benalcazar, Bernevig, and Hughes (BBH) [1,2] is an important model for the study of higher-order topological insulators [3–41]. It exhibits a quadrupole insulator phase with quantized bulk multipole moments. This phase is characterized by corner states carrying fractional corner charges $\pm e/2$, generalizing the bulk-boundary correspondence to higher order. The basic construction unit of quadrupole insulators is the Su-Schrieffer-Heeger (SSH) model [42]. The SSH model possesses quantized dipole moments in the bulk. Since a quadrupole consists of two separated dipoles, one may couple the SSH models in a particular way to obtain quantized quadrupole moments in the two-dimensional (2D) bulk. However, direct coupling of one-dimensional (1D) SSH chains from two directions does not work. It results in a gapless 2D SSH model with topological properties [43,44]. To get an insulating phase with quantized quadrupole moments, the indispensable ingredients are π fluxes threading each plaquette of the entire 2D lattice. The π-flux pattern generates an insulating phase at half filling. It projectively modifies the mirror symmetry M_x and M_y from commuting $[M_x, M_y] = 0$ to anticommuting $\{M_x, M_y\} = 0$. This change results in a BBH model with quantized bulk quadrupole moments [1,2].

In our work, we vary the π-flux pattern of the BBH model. This modification gives rise to a class of models that we call Klein-bottle BBH models. The name stems from the shape of the fundamental domain of momentum space being modified from a torus to a Klein bottle in mathematics by particular π-flux patterns [45–57]. In the first type of Klein-bottle BBH model, the π fluxes are applied only at the even numbered columns of plaquettes in the 2D SSH lattice [see Fig. 1(a)]. This model supports nontrivial Klein-bottle quadrupole insulator phases with corresponding boundary signatures such as quantized edge polarizations and fractional corner charges. We show that the nontrivial Klein-bottle quadrupole insulator is robust against flux perturbations. In the second type of Klein-bottle BBH model, we instead apply π fluxes at the odd numbered columns of plaquettes [see Fig. 7(a) below]. This subtle difference in π-flux patterns dramatically changes the phase diagram of the system. The second model does not support nontrivial Klein-bottle quadrupole insulators anymore. It shares some features with the first model, such as the twined edge modes and corner-localized charges, but its insulator phase is trivial with vanishing bulk quadrupole moments. Interestingly, we identify emergent Klein-bottle Dirac semimetal phases in both models, characterized by the coexistence of twined edge modes and bulk Dirac points. In particular, four Dirac points are located at high-symmetry points of the Brillouin zone (BZ). They are related by glide-mirror symmetry in momentum space. There are no such Dirac semimetal phases in the original BBH model.

This paper is organized as follows. In Sec. II, we present the first Klein-bottle BBH model, with an emphasis on the nontrivial Klein-bottle quadrupole insulator phase. In Sec. III, we study Klein-bottle Dirac semimetal phases. In Sec. IV, we show the robustness of Klein-bottle quadrupole insulators against flux variations. In Sec. V, we consider the properties of the second Klein-bottle BBH model with a different π-flux

*Corresponding author: changan.li@uni-wuerzburg.de

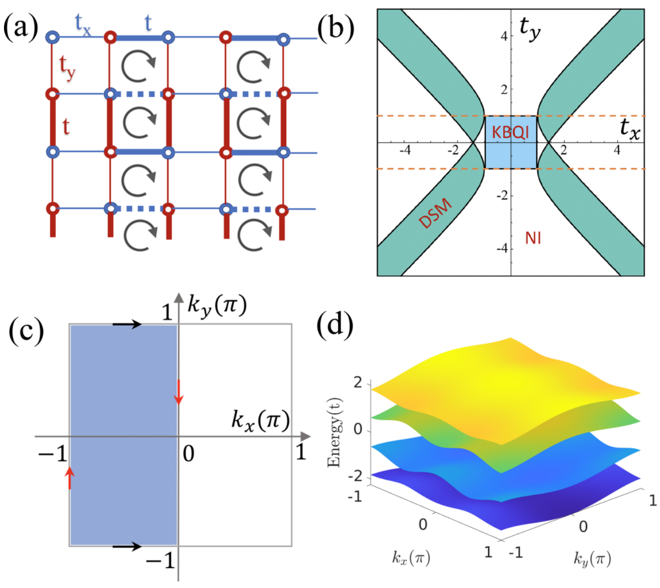

FIG. 1. (a) Sketch of the lattice for the first Klein-bottle BBH model with a specific π-flux pattern. The dashed lines indicate a negative sign to account for the π fluxes. (b) Phase diagram in the parameter space (t_x, t_y). The light blue region indicates the nontrivial Klein-bottle quadrupole insulators (KBQI); the light green region indicates the Dirac semimetal (DSM) phase. The region between the two dashed lines represents phases with nontrivial Klein-bottle topology. Other regions are normal insulators (NI). (c) Fundamental domain of momentum space in the BZ (blue). The boundaries marked with the same colored arrows should be identified in that sense and thus a Klein bottle. (d) Band structure for the first Klein-bottle BBH model in the insulating phase. There are four nondegenerate bands. The parameters are taken as $t_x = 0.6$ and $t_y = 0.3$ in units of t.

pattern. Finally, we conclude our results with a discussion in Sec. VI.

II. KLEIN-BOTTLE QUADRUPOLE INSULATORS INDUCED BY $\mathbb{Z}_2$ GAUGE FIELDS

A. The first Klein-bottle BBH model

We consider the first model as sketched in Fig. 1(a). Compared with the original BBH model, there are no uniform π fluxes in the whole 2D lattice. The π fluxes apply only at the even numbered columns of the plaquettes. The tight-binding Hamiltonian reads

$$\begin{aligned}H_1 = \sum_{\mathbf{R}} [&t_x(C^\dagger_{\mathbf{R},1}C_{\mathbf{R},3} + C^\dagger_{\mathbf{R},2}C_{\mathbf{R},4})\\ &+ t_y(C^\dagger_{\mathbf{R},1}C_{\mathbf{R},4} + C^\dagger_{\mathbf{R},2}C_{\mathbf{R},3})\\ &+ (-tC^\dagger_{\mathbf{R},1}C_{\mathbf{R}+\hat{x},3} + tC^\dagger_{\mathbf{R},4}C_{\mathbf{R}+\hat{x},2})\\ &+ t(C^\dagger_{\mathbf{R},1}C_{\mathbf{R}+\hat{y},4} + C^\dagger_{\mathbf{R},3}C_{\mathbf{R}+\hat{y},2})] + \text{H.c.},\end{aligned} \tag{1}$$

where $t_{x/y}$ and t are the corresponding hopping amplitudes along the x and y directions, as indicated in Fig. 1(a). The operators $C^\dagger_{\mathbf{R},\zeta}$ $(C_{\mathbf{R},\zeta})$ are creation (annihilation) operators at unit cell $\mathbf{R}$, with $\zeta \in \{1, 2, 3, 4\}$ being orbital degrees of freedom. Note that the minus sign from the π fluxes is encoded in the term $-tC^\dagger_{\mathbf{R},1}C_{\mathbf{R}+\hat{x},3} + \text{H.c.}$ We set the lattice constant as $a = 1$. In momentum space, the corresponding Bloch Hamiltonian reads

$$\begin{aligned}H_1(\mathbf{k}) = &t_x\tau_1\sigma_0 + [-t\cos k_x\gamma_3 + t\sin k_x\gamma_4\\ &+ (t_y + t\cos k_y)\gamma_1 - t\sin k_y\gamma_2],\end{aligned} \tag{2}$$

where $\gamma_j = \tau_1\sigma_j$ and $\gamma_4 = \tau_2\sigma_0$ are the gamma matrices. The Pauli matrices τ and σ correspond to different orbital degrees of freedom in the unit cell; $\mathbf{k} = (k_x, k_y)$ is the momentum in two dimensions. Different from the original BBH model, in addition to the four anticommuting Dirac matrices in Eq. (2), there is an extra term, $t_x\tau_1\sigma_0$. The Hamiltonian respects chiral symmetry $\gamma_5 H_1(\mathbf{k})\gamma_5^{-1} = -H_1(\mathbf{k})$, with the chiral symmetry operator defined as $\gamma_5 \equiv -\gamma_1\gamma_2\gamma_3\gamma_4 = \tau_3\sigma_0$. It has time-reversal symmetry $\mathcal{T}H_1(\mathbf{k})\mathcal{T}^{-1} = H_1(-\mathbf{k})$ as well, where $\mathcal{T} = K$ is just the complex conjugate operation. Therefore, particle-hole symmetry is also preserved.

With the help of chiral symmetry, the energy spectra can be obtained as

$$E^\pm_\eta(\mathbf{k}) = \pm\sqrt{\epsilon^2_y(k_y) + t^2 + t_x^2 + 2\eta t_x\sqrt{\epsilon^2_y(k_y) + t^2\cos^2 k_x}}, \tag{3}$$

where $\epsilon^2_y(k_y) \equiv t_y^2 + 2t_y t\cos k_y + t^2$ and $\eta = \pm 1$. The two lower (upper) bands are no longer degenerate unless $t_x = 0$ [see Fig. 1(d)]. We find that there are insulating phases as well as semimetal phases, as shown in the phase diagram in Fig. 1(b), different from that in the BBH model. We focus on the insulating phases in this section and delegate the discussion of the semimetal phases to Sec. IV.

B. Klein-bottle nontrivial phases, glide edge spectra, and Wannier bands

Due to the gauge degrees of freedom from π fluxes, the hopping amplitudes are allowed to take phases of ± 1. Thus, the π fluxes endow the system with a $\mathbb{Z}_2$ gauge field. This gauge field can projectively modify the algebra of certain symmetry operators [58]. The Klein-bottle BBH model has mirror symmetry along the x direction as $\mathcal{M}_x H_1(\mathbf{k})\mathcal{M}_x = H_1(-k_x, k_y)$, with $\mathcal{M}_x = \tau_1\sigma_0$. However, along the y direction, the system does not have exact mirror symmetry; it has mirror symmetry only after a gauge transformation acting on the $\mathbb{Z}_2$ gauge fields [2]. That is, $\mathcal{M}_y = G(M_y)M_y$ with a gauge transformation $G(M_y)$. However, we see that the gauge transformation $G(M_y)$ is not compatible with the translation operation $\mathcal{L}_x$. The relation between $\mathcal{M}_y$ and $\mathcal{L}_x$ becomes projectively modified as $\{\mathcal{M}_y, \mathcal{L}_x\} = 0$ due to $\mathbb{Z}_2$ gauge fields [45], instead of $[\mathcal{M}_y, \mathcal{L}_x] = 0$ without the gauge field. This fundamental change in the commutation relation introduces nonsymmorphic symmetry in momentum space and makes the fundamental domain of momentum space a Klein bottle [45]. Specifically, we find

$$\mathcal{M}_y H_1(\mathbf{k})\mathcal{M}_y^{-1} = H_1(k_x + \pi, -k_y), \tag{4}$$

where $\mathcal{M}_y = \tau_1\sigma_1$ in the chosen basis. This corresponds to glide-mirror symmetry in momentum space. Hence, the momentum at (k_x, k_y) is equivalent to $(k_x + \pi, -k_y)$. Consequently, the original BZ (torus) is reduced to two equivalent

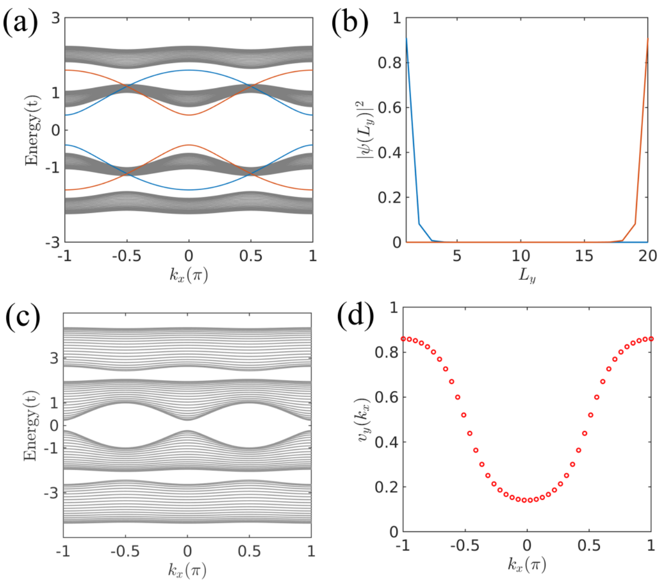

FIG. 2. (a) Spectra of a ribbon along the x direction. The blue and red lines indicate the twined edge modes. (b) Wave function distribution of the twined edge modes along the y direction of the ribbon. (c) Similar to (a), but in a topological trivial case without edge modes. (d) The Wannier spectrum $\nu_y(k_x)$ of the lowest energy band. The parameters are taken as $t_x = 0.6, t_y = 0.3$ for (a), (b), and (d) and $t_x = 1.2, t_y = 2$ for (c) in units of t.

fundamental domains [Klein bottles in Fig. 1(c)]. In the following, we use the term *Klein-bottle BZ* to indicate the fundamental domain of momentum space.

Consider a ribbon geometry along the x direction with open boundary conditions along the y direction. We find that there are edge modes residing within the bulk bands. If we resolve their spatial distributions, we find that the two pairs of edge modes emerge at different boundaries. Similar to those in the BBH model, those edge modes are gapped, as shown in Figs. 2(a) and 2(b). However, there are essential differences. The two pairs of edge spectra have a relative momentum shift $\delta k_x = \pi$, which is due to the glide-mirror symmetry, as stated above. Due to the relative momentum shift $\delta k_x = \pi$, two branches of edge modes from different pairs twine around each other from $k_x = -\pi$ to $k_x = \pi$. We call them *twined edge modes*. Moreover, the edge spectra cross the bulk continuum without hybridization. The energy spectra of the twined edge modes can be obtained as [29,59]

$$E_{\mathrm{b}}(k_x) = \pm\sqrt{t_x^2 + t^2 + 2t_x t\cos(k_x + \theta)}, \tag{5}$$

where $\theta = 0/\pi$ parametrizes the two different pairs of edge modes.

The existence of twined edge modes can be attributed to a topological invariant. In Ref. [45], the corresponding topological invariant is defined at the boundary of the Klein-bottle BZ as $w = \frac{1}{2\pi}[\gamma_y(k_x = 0) + \gamma_y(k_x = \pi)] \bmod 2$, where $\gamma_y(k_x)$ is the Berry phase for the reduced 1D Hamiltonian $h(k_y)$ at a specific k_x. This topological invariant is closely related to 1D charge polarization [45]. Note that this invariant becomes ill defined once the Klein-bottle BZ is broken. This happens when the value of magnetic flux deviates from π because in that case the relation $\{\mathcal{M}_y, \mathcal{L}_x\} = 0$ does not hold anymore. However, the twined edge modes, which serve as a practical indicator of Klein-bottle insulators, may survive under such flux deviations.

We alternatively employ the method of Wilson loops to characterize the topology of Klein-bottle phases. At half filling, we find that the bulk polarization of the system vanishes. Since the two lowest bands are not degenerate in this model and the twined edge modes reach the gap between these two bands, we consider the polarization of the *lowest* energy band (similar results can be obtained for the second band). We consider a ribbon geometry along the x direction. Thus, the bulk polarization p_y^κ along the y direction determines the existence of twined edge modes. In the nontrivial phase with $p_y^\kappa = \frac{1}{2}$, there are twined edge modes. In the trivial phase with $p_y^\kappa = 0$, no edge modes exist. The polarization p_y^κ is closely related to the Wannier center. We obtain the Wannier center from the Wilson loop method. To this end, we define the Wilson loop along the y direction at specific k_x in the Klein-bottle BZ, i.e., $W_y(k_x)$. Then the eigenvalues of $W_y(k_x)$ yield the Wannier center $\nu_y(k_x)$. The Wannier center indicates the average position of electrons relative to the center of the unit cell. The set of Wannier centers along the y direction as a function of k_x forms the Wannier bands $\nu_y(k_x)$. The topological invariant for the Klein-bottle insulator can be defined as

$$p_y^\kappa = \frac{2}{L_x}\sum_{k_x=-\pi}^{0}\nu_y(k_x), \tag{6}$$

which is the bulk polarization of the lowest energy band. Note that we can take the sum with respect to k_x from $-\pi$ to 0. The other range from 0 to π can be obtained by symmetry. Here, L_x is the number of unit cells in the x direction. The topological invariant p_y^κ should not be changed by flux perturbations as long as chiral symmetry is preserved.

The Wannier band $\nu_y(k_x)$ for the lowest energy band is plotted in Fig. 2(d). For the nontrivial Klein-bottle insulator phase, the Wannier band $\nu_y(k_x)$ has to cross $\nu_y = \frac{1}{2}$. Due to the periodicity of the BZ, $\nu_y(k_x)$ crosses $\nu_y = \frac{1}{2}$ an even number of times. Therefore, we obtain the bulk polarization $p_y^\kappa = \frac{1}{2}$ from the lowest energy bands as a topological invariant for Klein-bottle insulators. Note that the Wannier band crosses $\nu_y = \frac{1}{2}$ once within the domain $k_x \in [0, \pi]$, consistent with the winding number defined in Ref. [45]. For the trivial insulator case, it does not cross the value $\nu_y = \frac{1}{2}$ at all; thus, $p_y^\kappa = 0$.

We emphasize that at $k_x = \pm\frac{\pi}{2}$, the Wannier center is fixed at 0 or $\frac{1}{2}$. This is because at these special points the Hamiltonian $H_1(\pm\frac{\pi}{2}, k_y)$ has space-time inversion symmetry, which can quantize the Wannier center [60]. From the topological invariant p_y^κ, we find that the nontrivial Klein-bottle phase exists for

$$|t_y| < 1 \quad \Rightarrow \mathrm{p}_{\mathrm{y}}^\kappa = \tfrac{1}{2}, \tag{7}$$

as indicated in Fig. 1(b). Note that this phase regime contains Klein-bottle insulators (an insulating phase characterized by twined edge modes) and Klein-bottle Dirac semimetals (semimetals with twined edge modes).

C. Nontrivial Klein-bottle quadrupole insulators

Twined edge modes exist in the nontrivial Klein-bottle phases as a consequence of first-order topology. In our model, the twined edge modes are gapped as well. However, there is a relative momentum shift of the spectra at different edges. These spectra can touch, cross, or be hidden in the bulk continuum. An intriguing question is whether such twined edge modes can support second-order topology, characterized by corner states and fractional charges.

To characterize the system, we first calculate the quadrupole moment q_{xy}. Afterwards, we check the corresponding edge and corner signatures. The quadrupole moment can be obtained in real space as [18,29,34,61,62],

$$q_{xy} = \frac{1}{2\pi}\mathrm{Im}\log[\det(U^\dagger \hat{Q} U)\sqrt{\det(Q^\dagger)}], \tag{8}$$

where $\hat{Q} \equiv \exp[i2\pi\hat{q}_{xy}]$, with $\hat{q}_{xy} = \hat{x}\hat{y}/(L_xL_y)$ being the quadrupole momentum density operator per unit cell at position $\mathbf{R} = (x, y)$. Here, $\hat{x}$ ($\hat{y}$) is the position operator along the x (y) direction, and $L_{x(y)}$ is the corresponding system size. The matrix U is constructed by packing all the occupied eigenstates in a columnwise way. The quantization of q_{xy} is protected by chiral symmetry [29,34]. For an insulating phase, it is a nontrivial quadrupole insulator when $q_{xy} = \frac{1}{2}$. We find the nontrivial Klein-bottle quadrupole insulator phase in the regime $|t_x| < 1$ and $|t_y| < 1$ [see Fig. 1(b)], similar to the BBH model.

The edge polarizations p_x^{edge} and p_y^{edge} can also help us to detect the topologically nontrivial phase. Take p_x^{edge} as an example. Consider a ribbon along the x direction with width L_y along the y direction. With the Wilson loop method, the edge polarization is calculated as [1,2,32]

$$p_x^{\mathrm{edge}} = \sum_{y=1}^{L_y/2} p_x(y), \tag{9}$$

where $p_x(y)$ is the distribution of polarization along the y direction. We calculate this spatially resolved polarization as

$$p_x(y) = \sum_{j=1}^{2L_y} \rho^j(y)\nu_y^j(k_x), \tag{10}$$

where $\rho^j(y) = \frac{1}{L_x}\sum_{k_x,\zeta}|\sum_n [u_{k_x}^n]^{y,\zeta}[\nu_{k_x}^j]^n|^2$. Here, $[\nu_{k_x}^j]^n$ is the nth component of the jth Wilson loop eigenstate $|\nu_{k_x}^j\rangle$ corresponding to the eigenvalue $\nu_y^j(k_x)$, while $[u_{k_x}^n]_{y,\zeta}$ is the nth eigenstate of the Hamiltonian $H_y(k_x)$ on the ribbon with integer number $n \in \{1, 2, 3, \ldots, 2L_y\}$. The edge polarization p_y^{edge} in the y direction can be calculated in a similar way. For a nontrivial quadrupole insulator, $(p_x^{\mathrm{edge}}, p_y^{\mathrm{edge}}) = (\frac{1}{2}, \frac{1}{2})$.

Consider a ribbon along the x direction with open boundaries in the y direction. In Figs. 3(a) and 3(b), two topological states are localized on the edge with half-integer Wannier values, while the other states are distributed over the bulk. The edge polarization $p_x(y)$ becomes nonzero at the sample edge. The spatially resolved polarization yields quantized edge polarization $p_x^{\mathrm{edge}} = \frac{1}{2}$ ($p_y^{\mathrm{edge}} = \frac{1}{2}$). Similar results appear for a ribbon along the y direction, as shown in Figs. 3(c) and 3(d).

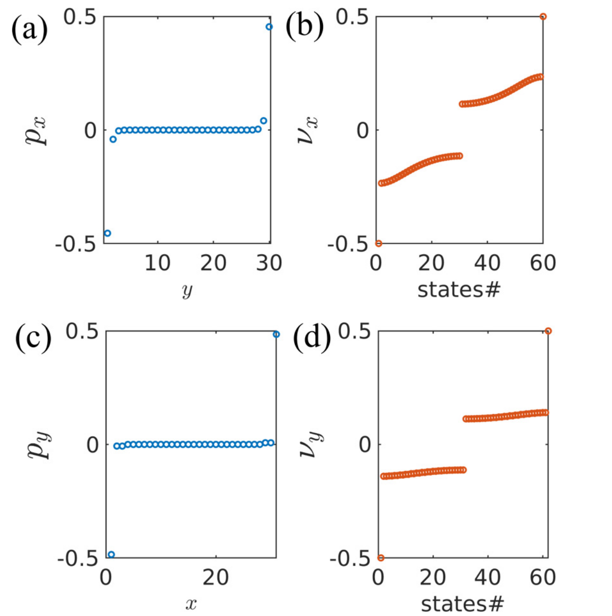

FIG. 3. (a) Edge polarization p_x along y. (b) Wannier center ν_x for different eigenstates. (c) Edge polarization p_y along x. (d) Wannier center ν_y for different eigenstates. The parameters are taken as $t_x = 0.6, t_y = 0.3$ in units of t.

Moreover, there are zero-energy corner modes carrying fractional corner charges. We show in Fig. 4(a) that there are fourfold-degenerate zero-energy modes whose wave functions are sharply localized at corners of the sample. It is also found that the corner charges are fractionalized at $\pm e/2$ [see Fig. 4(b)].

III. KLEIN-BOTTLE DIRAC SEMIMETALS ON SQUARE LATTICES

Besides the Klein-bottle insulating phase, a Dirac semimetal phase also exists, as shown in Fig. 5. There are four Dirac points residing in the BZ. From the energy band solutions in Eq. (3), to obtain band touching at zero energy (due to chiral symmetry), we require $\cos^2 k_x = 1$, i.e., $k_x \in \{0, \pi\}$.

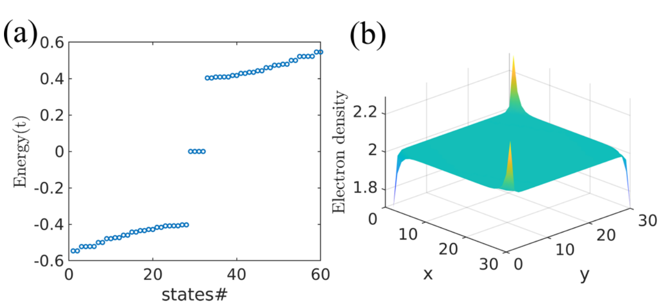

FIG. 4. (a) Energy spectrum of the model with open boundaries in both direction. There are four zero-energy corner modes at zero energy. (b) Electron charge density distribution on the lattice. It gives fractional corner charges $\pm\frac{e}{2}$. The parameters are taken as $t_x = 0.6, t_y = 0.3$ in units of t.

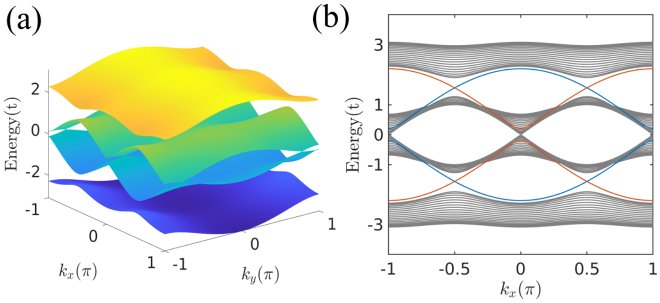

FIG. 5. (a) Four Dirac points in the band structure. (b) Coexistence of edge Dirac points and bulk edge Dirac points in the spectra of a ribbon along the x direction. The parameters are taken as $t_x = 1.2, t_y = 0.6$ in units of t.

In this case, the energy spectra are simplified as

$$E_\eta^\pm(\mathbf{k}) = \pm\Big(\sqrt{\epsilon_y^2(k_y) + t^2} + 2\eta t_x\Big). \tag{11}$$

Therefore, four Dirac points are located at

$$(K_x, K_y) = \left(0/\pi, \ \pm\arccos\left[\frac{t_x^2 - t_y^2 - 2t^2}{2t_y t}\right]\right). \tag{12}$$

The valid solutions for K_y give rise to the Klein-bottle Dirac semimetal phase, determined by the overlap of two hyperbolas in the parameter space (t_x, t_y) as

$$(t_y \pm t)^2 - t_x^2 = t^2, \tag{13}$$

as shown in Fig. 1(b). The Dirac semimetal phase that appears in this model has no counterpart in the original BBH model.

The Dirac points are located at the boundary of the Klein-bottle BZ. They come in two dual pairs related by glide-mirror symmetry $\mathcal{M}_y$ as $\{(0, \pm K_y) \Leftrightarrow (\pi, \mp K_y)\}$. We know that the topological protection of Dirac points is typically related to a winding number defined on a path enclosing the Dirac points. Due to chiral symmetry, rewriting the Hamiltonian Eq. (2) in an off-diagonal form leads to

$$H_1(\mathbf{k}) = \begin{pmatrix} 0 & q(\mathbf{k}) \\ q^\dagger(\mathbf{k}) & 0 \end{pmatrix}, \tag{14}$$

where

$$q(\mathbf{k}) = \begin{pmatrix} -t_x + te^{ik_x} & t_y + te^{ik_y} \\ t_y + te^{-ik_y} & t_x + te^{-ik_x} \end{pmatrix}. \tag{15}$$

The winding number for the Dirac points is defined as $\omega = \frac{1}{2\pi i}\oint_\ell d\mathbf{k}\cdot \mathrm{Tr}[q^{-1}(\mathbf{k})\nabla_\mathbf{k} q(\mathbf{k})]$ [63,64], where the loop ℓ is chosen such that it encloses a single Dirac point.

The twined edge modes from nontrivial Klein-bottle topology also appear in the Dirac semimetal phase, as shown in the Fig. 5(b). The bulk Dirac points coexist with edge Dirac points, located at different energies. For certain parameters, they are hidden in the bulk bands but do not directly merge with the continuum. From the wave function distribution, we find that the edge modes are well localized at boundaries even if they coexist with bulk bands. In the Dirac semimetal phase with a trivial Klein-bottle topology for $|t_y| > 1$, the twined edge modes disappear.

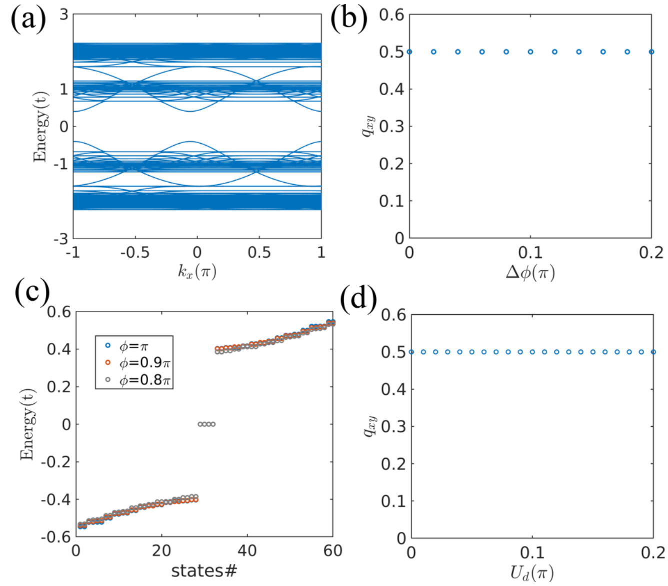

FIG. 6. (a) Energy spectrum on a ribbon along the x direction when $\phi = 0.95\pi$. (b) Quadrupole moment q_{xy} as a function of flux deviation $\Delta\phi = \pi - \phi$. (c) Eigenstates around zero energy for different $\Delta\phi$. (d) Quadrupole moment q_{xy} as a function of random flux strength U_d. The parameters are taken as $t_x = 0.6$, $t_y = 0.3$ in units of t.

IV. ROBUSTNESS OF NONTRIVIAL QUADRUPOLE INSULATORS AGAINST FLUX PERTURBATIONS

In the previous section, we showed that the realization of Klein-bottle quadrupole insulators relies on exact threading of π fluxes on even numbers of plaquettes in the 2D lattice. We now address the question of how robust nontrivial Klein-bottle quadrupole insulators are against flux deviations from the value of π. We check the stability of the nontrivial Klein-bottle quadrupole insulators in two cases: In the first one, the flux ϕ deviates from π but is still uniform in the lattice. This helps us to determine how general the nontrivial phases are. In the second one, the flux value is chosen randomly, fluctuating around π.

A. Uniform flux deviations

Let us first check the evolution of twined edge modes for a model with flux ϕ deviating from π uniformly. In the original case, the well-localized twined edge modes cross the bulk bands without hybridization [Fig. 2(a)]. When $\phi = 0.95\pi$, the twined edge modes almost keep their form [Fig. 6(a)], but the overlapping parts start to hybridize. In this case, the Klein-bottle BZ manifold is broken because the glide-mirror symmetry does not hold anymore. We define $\Delta\phi = \pi - \phi$. As $\Delta\phi$ increases further, the twined edge modes hybridize with the other bands stronger. This may be explained as the hybridization of Landau levels (flat bands) and twined edge modes.

Now, we check the robustness of Klein-bottle quadrupole insulators against flux perturbations. To this end, we employ the quadrupole moments q_{xy} and the corresponding corner states. To be specific, we take $t_x = 0.6$ and $t_y = 0.3$ in the

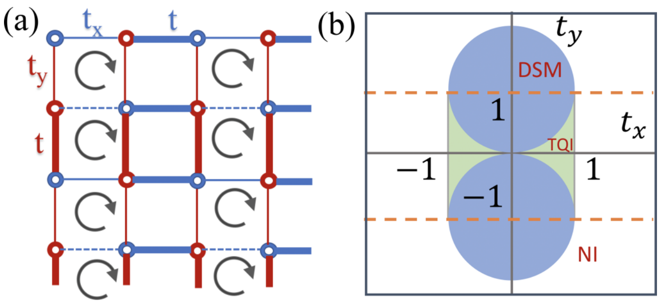

FIG. 7. (a) Sketch of the lattice for the second Klein-bottle BBH model with a different π-flux pattern. The dashed lines indicate a negative sign to account for the π fluxes. (b) Phase diagram in the parameter space (t_x, t_y). The light blue region indicates the Dirac semimetal (DSM) phase; the light green region indicates the trivial quadrupole insulators (TQI). The region between the two dashed lines represent phases with nontrivial Klein-bottle topology. Other regions are the normal insulators (NI).

calculations. Figure 6(b) demonstrates that q_{xy} stays at $q_{xy} = \frac{1}{2}$ even if $\Delta\phi$ grows to a relatively large value. This result indicates that the Klein-bottle quadrupole insulator is robust against flux deviations. It also suggests that nontrivial quadrupole insulators exist in an extended range of flux values ϕ, not just at $\phi = \pi$. Correspondingly, there are four zero-energy corner states in the gap of the spectrum [see Fig. 6(c)] with quantized fractional charge at each corner. The robustness of nontrivial Klein-bottle quadrupole insulators can be attributed to the persistence of twined edge modes under flux perturbations. They remain almost intact and gapped [Fig. 6(a)].

B. Random flux

The magnetic flux can also be chosen randomly at each plaquette [65]. We assume that the magnetic flux ϕ fluctuates around π. The flux deviation at each plaquette takes a random value from the uniformly distributed range $[-U_d, U_d]$, with U_d being a disorder strength. We also check the quadrupole moments q_{xy} under random flux. From Fig. 6(d), q_{xy} remains at $\frac{1}{2}$ as U_d increases from 0 up to 0.2π. When calculating q_{xy}, we can also investigate a single disorder configuration. We then find that the zero-energy midgap states and corner charges remain robust. Together with q_{xy}, these findings suggest strong robustness of nontrivial quadrupole insulators against random flux.

V. TRIVIAL KLEIN-BOTTLE QUADRUPOLE INSULATORS WITH CORNER STATES

Now, we consider the second Klein-bottle BBH model sketched in Fig. 7(a). The π fluxes apply only to the odd numbered columns of plaquettes, instead of the even numbered columns. This subtle change in applying π-flux patterns makes a strong difference. It gives rise to a totally different Hamiltonian. The nontrivial quadrupole insulators do not appear anymore. There are also insulators and Dirac semimetals in the phase diagram [Fig. 7(b)], but the insulator is a trivial insulator with $q_{xy} = 0$, although it supports corner charges.

The tight-binding Hamiltonian of the second Klein-bottle BBH model reads

$$\begin{aligned} H_2 = \sum_{\mathbf{R}} [(&-t_x C^\dagger_{\mathbf{R},1} C_{\mathbf{R},3} + t_x C^\dagger_{\mathbf{R},2} C_{\mathbf{R},4}) \\ &+ t_y (C^\dagger_{\mathbf{R},1} C_{\mathbf{R},4} + C^\dagger_{\mathbf{R},2} C_{\mathbf{R},3}) \\ &+ t (C^\dagger_{\mathbf{R},1} C_{\mathbf{R}+\hat{x},3} + C^\dagger_{\mathbf{R},4} C_{\mathbf{R}+\hat{x},2}) \\ &+ t (C^\dagger_{\mathbf{R},1} C_{\mathbf{R}+\hat{y},4} + C^\dagger_{\mathbf{R},3} C_{\mathbf{R}+\hat{y},2})] + \text{H.c.}, \end{aligned} \tag{16}$$

where the minus sign from the π fluxes is taken into account in the term $-t_x C^\dagger_{\mathbf{R},1} C_{\mathbf{R},3} + \text{H.c.}$ In momentum space, the Bloch Hamiltonian corresponding to Eq. (16) becomes

$$\begin{aligned} H_2(\mathbf{k}) = &- t_x \tau_1 \sigma_3 + t \cos k_x \tau_1 \sigma_0 - t \sin k_x \tau_2 \sigma_3 \\ &+ (t_y + t \cos k_y) \tau_1 \sigma_1 - t \sin k_y \tau_1 \sigma_2. \end{aligned} \tag{17}$$

The bulk spectrum of Eq. (17) reads

$$E^{\pm}_\eta(\mathbf{k}) = \pm \sqrt{\epsilon^2_y(k_y) + t^2 + t^2_x + 2\eta t \sqrt{\epsilon^2_y(k_y) + t^2_x \cos^2 k_x}}, \tag{18}$$

where $\epsilon^2_y(k_y) \equiv t^2_y + 2 t_y t \cos k_y + t^2$ is defined in the same way as before. This model also respects chiral symmetry $\gamma_5 H_1(\mathbf{k}) \gamma_5^{-1} = -H_1(\mathbf{k})$. The π-flux gauge field gives rise to nonsymmorphic symmetry in momentum space as

$$\mathcal{M}'_y H_2(\mathbf{k}) \mathcal{M}'^{-1}_y = H_2(k_x + \pi, -k_y), \tag{19}$$

where $\mathcal{M}'_y = \tau_2 \sigma_2$ in the chosen basis.

The phase diagram of the second Klein-bottle BBH model is plotted in Fig. 7(b). The Dirac semimetal phase is located inside the two circles in parameter space (t_x, t_y),

$$t^2_x + (t_y \pm t)^2 = t^2. \tag{20}$$

The Dirac points are at

$$(K_x, K_y) = \left(0/\pi, \quad \pm \arccos\left[-\frac{t^2_x + t^2_y}{2 t_y t}\right]\right). \tag{21}$$

In the Klein-bottle Dirac semimetal phases, there are twined edge modes on a ribbon geometry with an open boundary. The other regions are insulating phases. The nontrivial Klein-bottle phase is bounded by $|t_y| < 1$. Compared with the first model in Eq. (2), the different π-flux pattern in the second Klein-bottle BBH model leads to totally different matrix structures in Eq. (17). Thus, the corresponding energy bands are quite different, giving rise to significantly different phase diagrams. Moreover, we notice the exchange of variables $t \longleftrightarrow t_x$ in the energy bands compared to Eq. (3). This can be effectively viewed as the exchange of dimerized hopping strength of the SSH model along the x direction, which makes the topological properties different from those of the first model.

In an insulator phase, we find that the edge polarizations take the values $(p^{\text{edge}}_x, p^{\text{edge}}_y) = (\frac{1}{2}, 0)$. This anisotropic property of edge polarizations bears similarity to weak topological insulators. In Fig. 8(a), we plot the edge polarizations p^{edge}_y, together with the Wannier values of eigenstates. The edge polarization p^{edge}_y is zero [the nontrivial $p^{\text{edge}}_x = \frac{1}{2}$ is not shown here].

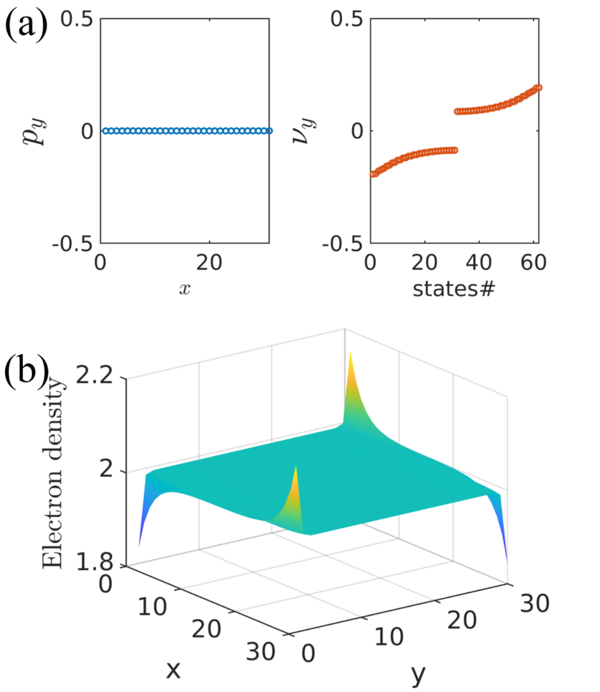

FIG. 8. (a) Edge polarization p_y along x (left panel) and the Wannier center ν_y for different eigenstates (right panel) in the second Klein-bottle BBH model. (b) Electron density distribution in the lattice. The parameters are taken as $t_x = 0.8, t_y = 0.2$ in units of t for all plots.

Consider open boundary conditions along both the x and y directions. Then, the edge polarizations are terminated at corners. This leads to charges $Q^{\text{corner}} = \pm\frac{e}{2}$ localized at the corners [see Fig. 8(b)]. There are four zero-energy midgap states in the energy spectra when (t_x, t_y) is located in the light green region of the phase diagram in Fig. 7(b). However, if we calculate the topological invariant q_{xy}, we find that the second Klein-bottle BBH model is a trivial Klein-bottle insulator. Remarkably, it exhibits twined edge modes (first order) and corner-localized charges, but it has a vanishing quadrupole moment $q_{xy} = 0$ (second-order topological invariant). The defining properties of a quadrupole insulator $|q_{xy}| = |p_x^{\text{edge}}| = |p_y^{\text{edge}}| = |Q^{\text{corner}}|$ are not satisfied [2]. The corner charges follow $Q^{\text{corner}} = p_x^{\text{edge}} + p_y^{\text{edge}}$. Thus, the corner charges and edge polarizations are pure surface effects, unrelated to bulk quadrupole moments [2].

We further analyze the robustness of twined edge modes in the Klein-bottle phases when the magnetic flux deviates from π. Consider a ribbon along the x direction. In the Klein-bottle Dirac semimetal phases, the twined edge modes reside between the bulk bands and can be detached from them. When we gradually change ϕ from π, the twined edge modes persist and are detached from the bulk modes even up to a relatively large $\Delta\phi$, as shown in Fig. 9(b).

VI. DISCUSSION AND CONCLUSIONS

We showed that the variation of π-flux patterns changes the topology of the considered system dramatically. Hence, particular π-flux patterns may help us to search for novel

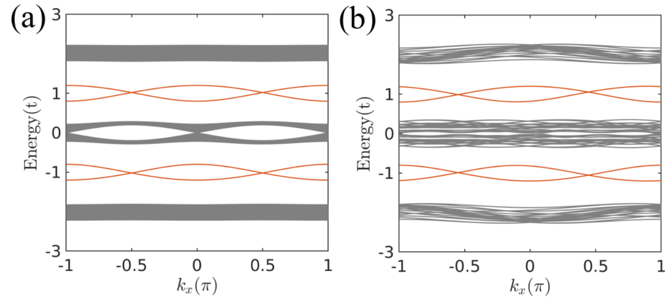

FIG. 9. (a) Energy spectrum of the second Klein-bottle BBH model on a ribbon along the x direction. The edge and bulk Dirac points coexist. (b) Same as (a), but with flux $\phi = 0.9\pi$. The parameters are taken as $t_x = t_y = 0.2$ in units of t.

topological phases. The Klein-bottle quadrupole insulator requires only half of the total π fluxes compared to the original BBH model, simplifying experimental realizations of nontrivial quadrupole insulators. The manipulation of magnetic flux is possible in different synthetic systems. Therefore, our predictions are experimentally relevant.

In summary, we have proposed the existence of nontrivial Klein-bottle quadrupole insulators and Dirac semimetals in two dimensions. The twined edge modes, which support the second-order topology, appear to be a characteristic signature of Klein-bottle systems. We have verified the robustness of the nontrivial quadrupole insulators against flux perturbations. In the Klein-bottle Dirac semimetal phases, we discovered the coexistence of edge Dirac points and bulk Dirac points.

ACKNOWLEDGMENTS

C.-A.L. thanks J. Budich and B. Fu for helpful discussions. This work was financially supported by the Würzburg-Dresden Cluster of Excellence ct.qmat, Project No. 390858490; the DFG (SFB 1170); and the Bavarian Ministry of Economic Affairs, Regional Development and Energy within the High Tech Agenda Project "Bausteine für das Quanten Computing auf Basis Topologischer Materialen." H.G. acknowledges support from NSFC Grant No. 12074022.

APPENDIX A: REVISITING THE KLEIN-BOTTLE INSULATOR MODEL

For a better understanding of our results, we revisit the Klein-bottle insulator proposed in Ref. [45]. The Hamiltonian in two dimensions reads

$$H_0(\mathbf{k}) = \begin{pmatrix} \epsilon & [q_1^x(k_x)]^* & [q_+^y(k_y)]^* & 0 \\ q_1^x(k_x) & \epsilon & 0 & [q_-^y(k_y)]^* \\ q_+^y(k_y) & 0 & -\epsilon & [q_2^x(k_x)]^* \\ 0 & q_-^y(k_y) & q_2^x(k_x) & -\epsilon \end{pmatrix}, \tag{A1}$$

where the parameters are defined as $q_\ell^x(k_x) = t_{\ell 1}^x + t_{\ell 2}^x e^{ik_x}$, with $\ell = 1, 2$ and $q_\pm^y(k_y) = t_1^y \pm t_2^y e^{ik_y}$. The staggered on-site potential $\pm\epsilon$ opens a band gap at the finite-energy Dirac points. The inclusion of the term $H'(\mathbf{k}) = \lambda \cos k_y \sigma_1 \tau_2 +$

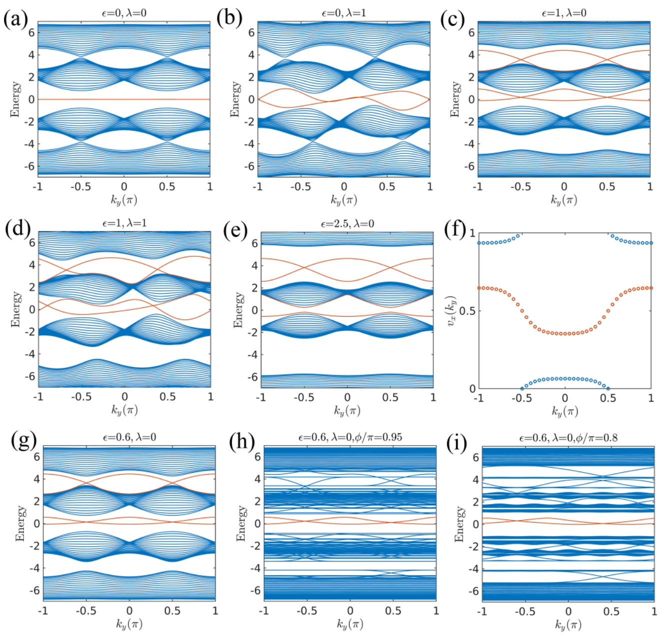

FIG. 10. (a)–(e) and (g) Energy spectra of the model specified in Eq. (A1) on a ribbon along the y direction. The red lines indicate the twined edge modes. (f) Wannier bands of the lowest energy band (blue) and the second energy band (red) corresponding to (c). (h) and (i) correspond to (g), but with the flux deviation from π. The other parameters are $t_{11}^x = t_{22}^x = 1$, $t_{12}^x = t_{21}^x = 3.5$, $t_1^y = 2$, and $t_2^y = 1.5$, the same as in Ref. [45]. The values of ϵ and λ are labeled on each plot.

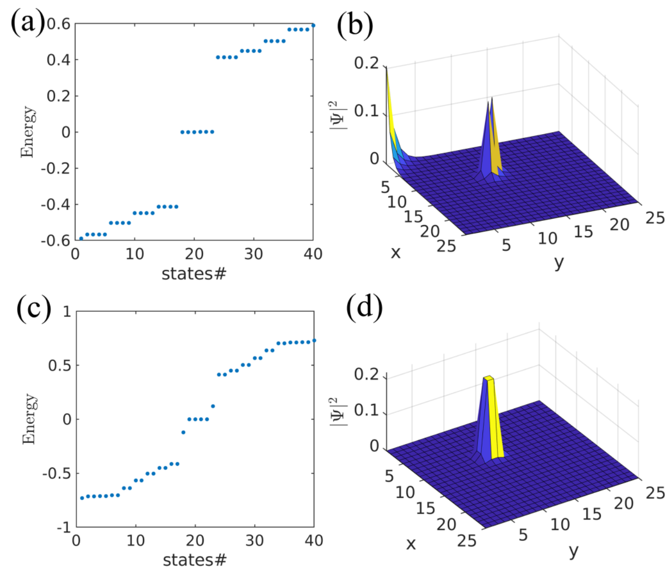

FIG. 11. (a) Energy spectra for the BBH model with a π-flux defect. There are six zero-energy modes in the gap in total in the topological nontrivial phase. The π-flux defect bounds two extra zero-energy modes. (b) The wave function distribution corresponds to the bound state in (a). Here, $t_x = t_y = 0.5$ for (a) and (b). (c) The same as (a), but the two bound states are away from zero energy. (d) The wave function distribution corresponds to the bound state in (c). Here, $t_x = 0.3$, $t_y = 0.6$ for (c) and (d).

$\lambda \sin k_y \sigma_2 \tau_2$ breaks time-reversal symmetry. In Fig. 10, we plot the spectrum of the model.

In the limit $\epsilon = 0$ and $\lambda = 0$, there is an energy gap close to zero energy. Then, Dirac points, formed by the first and second (third and fourth) bands, emerge. In this case, the nontrivial polarization gives zero-energy edge modes on a ribbon along the y direction [see Fig. 10(a)], similar to the zero-energy modes in zigzag graphene ribbons [66,67]. When considering the ribbon along the x direction, the energy spectrum shows a trivial gap without edge modes. This anisotropic property is the same as in the inclined 2D SSH model [44].

If we turn on the λ term, the flat edge modes become dispersive. If we turn on the on-site potential ϵ, we find the Dirac points at finite energy are gapped out. Then, there are two pairs of twined edge modes: one pair close to zero energy and the other pair at finite energy. The appearance of twined edge modes can be understood from the Wannier spectrum in Fig. 10(f). One branch of Wannier bands exhibits nontrivial winding around $\nu_x = \frac{1}{2}$, and the other one exhibits trivial winding around $\nu_x = 0$ instead. The total polarization is $p_x = \frac{1}{2}$.

In Fig. 10(d), we turn on both the λ and ϵ terms. This yields the same result as that shown in Ref. [45], but now we observe two pairs of twined edge modes within a larger energy window. Tuning the parameter ϵ, this can change the position of the twined edge modes [see Fig. 10(e)].

The twined edge modes also show robustness against flux perturbations. We consider a case in Fig. 10(g) in which one pair of twined edge modes is detached from the bulk bands close to zero energy and the other pair is attached to the bulk continuum at finite energy. When the flux gradually deviates from π, we find the detached twined edge modes persist in the spectra, as shown in Figs. 10(h) and 10(i). The other pair of edge modes at finite energy starts to hybridize with the bulk bands.

APPENDIX B: OVERVIEW OF THE BENALCAZAR-BERNEVIG-HUGHES MODEL

For the convenience of comparison with Klein-bottle BBH models presented in the main text, let us first briefly review the BBH model in two dimensions [1,2]. The tight-binding Hamiltonian in real space is described as

$$\begin{aligned} H_0 = \sum_{\mathbf{R}} [& t_x (C_{\mathbf{R},1}^\dagger C_{\mathbf{R},3} + C_{\mathbf{R},2}^\dagger C_{\mathbf{R},4}) \\ & + t_y (C_{\mathbf{R},1}^\dagger C_{\mathbf{R},4} - C_{\mathbf{R},2}^\dagger C_{\mathbf{R},3}) \\ & + t (C_{\mathbf{R},1}^\dagger C_{\mathbf{R}+\hat{x},3} + C_{\mathbf{R},4}^\dagger C_{\mathbf{R}+\hat{x},2}) \\ & + t (C_{\mathbf{R},1}^\dagger C_{\mathbf{R}+\hat{y},4} - C_{\mathbf{R},3}^\dagger C_{\mathbf{R}+\hat{y},2})] + \text{H.c.} \end{aligned} \quad \text{(B1)}$$

The corresponding Bloch Hamiltonian in momentum space is

$$H_0(\mathbf{k}) = [t_x + t\cos k_x]\Gamma_4 + t\sin k_x\Gamma_3 + [t_y + t\cos k_y]\Gamma_2 + t\sin k_y\Gamma_1. \tag{B2}$$

The gamma matrices are defined as $\Gamma_j \equiv -\tau_2\sigma_j$ and $\Gamma_4 \equiv \tau_1\sigma_0$. The bulk bands of Eq. (B2) are gapped unless $t_s/t = \pm 1$ ($s = x, y$). Hence, it is an insulator at half filling. The nonspatial symmetries of the BBH model are chiral symmetry, time-reversal symmetry, and particle-hole symmetry.

The nontrivial phase of the quadrupole insulator is characterized by quantized quadrupole moments $q_{xy} = \frac{1}{2}$, which induces quantized corner charge Q^{corner} and edge polarization p^{edge} of equal magnitude, $|q_{xy}| = |p_x^{\text{edge}}| = |p_y^{\text{edge}}| = |Q^{\text{corner}}|$. The quantization of q_{xy} relies on chiral symmetry [29,34]. The quadrupole insulators in two dimensions have boundaries that are stand-alone 1D topological insulators. The nontrivial topological quadrupole phase is located in the parameter region $|t_s/t| < 1$ [1,2].

APPENDIX C: STATES BOUND BY π-FLUX DEFECTS IN THE ORIGINAL BENALCAZAR-BERNEVIG-HUGHES MODEL

In this Appendix, we demonstrate that a single π-flux defect in the original BBH model may trap two bound states. The original BBH model needs π fluxes on all plaquettes of the 2D lattice. A π-flux defect means that at a specific plaquette the π flux is removed. Consider a single π-flux defect in the 2D BBH model lattice. In the nontrivial quadrupole insulator phase, the π-flux defect can induce bound states in the energy gap. As shown in Fig. 11(a), there are six zero-energy modes in total in the bulk gap: four of them are corner modes and the extra two are bound states at the π-flux defect. These two bound states are degenerate at zero energy. Their wave function is shown in Fig. 11(b). Another possibility is that the bound states have finite energy, as shown in Fig. 11(c). Their wave function localizes at the position of the π-flux defect [see Fig. 11(d)].

[1] W. A. Benalcazar, B. A. Bernevig, and T. L. Hughes, Quantized electric multipole insulators, Science **357**, 61 (2017).

[2] W. A. Benalcazar, B. A. Bernevig, and T. L. Hughes, Electric multipole moments, topological multipole moment pumping, and chiral hinge states in crystalline insulators, Phys. Rev. B **96**, 245115 (2017).

[3] J. Langbehn, Y. Peng, L. Trifunovic, F. von Oppen, and P. W. Brouwer, Reflection-symmetric second-order topological insulators and superconductors, Phys. Rev. Lett. **119**, 246401 (2017).

[4] Z. Song, Z. Fang, and C. Fang, $(d-2)$-dimensional edge states of rotation symmetry protected topological states, Phys. Rev. Lett. **119**, 246402 (2017).

[5] Y. Peng, Y. Bao, and F. von Oppen, Boundary Green functions of topological insulators and superconductors, Phys. Rev. B **95**, 235143 (2017).

[6] E. Khalaf, Higher-order topological insulators and superconductors protected by inversion symmetry, Phys. Rev. B **97**, 205136 (2018).

[7] M. Geier, L. Trifunovic, M. Hoskam, and P. W. Brouwer, Second-order topological insulators and superconductors with an order-two crystalline symmetry, Phys. Rev. B **97**, 205135 (2018).

[8] F. Schindler, Z. Wang, M. G. Vergniory, A. M. Cook, A. Murani, S. Sengupta, A. Yu. Kasumov, R. Deblock, S. Jeon, I. Drozdov, H. Bouchiat, S. Guéron, A. Yazdani, B. A. Bernevig, and T. Neupert, Higher-order topology in bismuth, Nat. Phys. **14**, 918 (2018).

[9] M. Serra-Garcia, V. Peri, R. Süsstrunk, O. R. Bilal, T. Larsen, L. G. Villanueva, and S. D. Huber, Observation of a phononic quadrupole topological insulator, Nature (London) **555**, 342 (2018).

[10] C. W. Peterson, W. A. Benalcazar, T. L. Hughes, and G. Bahl, A quantized microwave quadrupole insulator with topologically protected corner states, Nature (London) **555**, 346 (2018).

[11] S. Franca, J. van den Brink, and I. C. Fulga, An anomalous higher-order topological insulator, Phys. Rev. B **98**, 201114(R) (2018).

[12] F. Schindler, A. M. Cook, M. G. Vergniory, Z. Wang, S. S. P. Parkin, B. A. Bernevig, and T. Neupert, Higher-order topological insulators, Sci. Adv. **4**, eaat0346 (2018).

[13] M. Ezawa, Higher-order topological insulators and semimetals on the breathing kagome and pyrochlore lattices, Phys. Rev. Lett. **120**, 026801 (2018).

[14] G. van Miert and C. Ortix, Higher-order topological insulators protected by inversion and rotoinversion symmetries, Phys. Rev. B **98**, 081110(R) (2018).

[15] S. Imhof, C. Berger, F. Bayer, J. Brehm, L. W. Molenkamp, T. Kiessling, F. Schindler, C. H. Lee, M. Greiter, T. Neupert, and R. Thomale, Topolectrical-circuit realization of topological corner modes, Nat. Phys. **14**, 925 (2018).

[16] Z. Wang, B. J. Wieder, J. Li, B. Yan, and B. A. Bernevig, Higher-order topology, monopole nodal lines, and the origin of large Fermi arcs in transition metal dichalcogenides $X\mathrm{Te}_2$ ($X = \mathrm{Mo}, \mathrm{W}$), Phys. Rev. Lett. **123**, 186401 (2019).

[17] D. Călugăru, V. Juričić, and B. Roy, Higher-order topological phases: A general principle of construction, Phys. Rev. B **99**, 041301(R) (2019).

[18] B. Roy, Antiunitary symmetry protected higher-order topological phases, Phys. Rev. Res. **1**, 032048(R) (2019).

[19] B.-Y. Xie, G.-X. Su, H.-F. Wang, H. Su, X.-P. Shen, P. Zhan, M.-H. Lu, Z.-L. Wang, and Y.-F. Chen, Visualization of higher-order topological insulating phases in two-dimensional dielectric photonic crystals, Phys. Rev. Lett. **122**, 233903 (2019).

[20] M. J. Park, Y. Kim, G. Y. Cho, and S. B. Lee, Higher-order topological insulator in twisted bilayer graphene, Phys. Rev. Lett. **123**, 216803 (2019).

[21] W. A. Benalcazar, T. Li, and T. L. Hughes, Quantization of fractional corner charge in C_n-symmetric higher-order topological crystalline insulators, Phys. Rev. B **99**, 245151 (2019).

[22] R. Okugawa, S. Hayashi, and T. Nakanishi, Second-order topological phases protected by chiral symmetry, Phys. Rev. B **100**, 235302 (2019).

[23] X.-L. Sheng, C. Chen, H. Liu, Z. Chen, Z.-M. Yu, Y. X. Zhao, and S. A. Yang, Two-dimensional second-

order topological insulator in graphdiyne, Phys. Rev. Lett. **123**, 256402 (2019).

[24] R. Chen, C.-Z. Chen, J.-H. Gao, B. Zhou, and D.-H. Xu, Higher-order topological insulators in quasicrystals, Phys. Rev. Lett. **124**, 036803 (2020).

[25] A. K. Ghosh, G. C. Paul, and A. Saha, Higher order topological insulator via periodic driving, Phys. Rev. B **101**, 235403 (2020).

[26] Y. Ren, Z. Qiao, and Q. Niu, Engineering corner states from two-dimensional topological insulators, Phys. Rev. Lett. **124**, 166804 (2020).

[27] R.-X. Zhang, F. Wu, and S. Das Sarma, Möbius insulator and higher-order topology in $MnBi_{2n}Te_{3n+1}$, Phys. Rev. Lett. **124**, 136407 (2020).

[28] T. Hirosawa, S. A. Díaz, J. Klinovaja, and D. Loss, Magnonic quadrupole topological insulator in antiskyrmion crystals, Phys. Rev. Lett. **125**, 207204 (2020).

[29] C.-A. Li, B. Fu, Z.-A. Hu, J. Li, and S.-Q. Shen, Topological phase transitions in disordered electric quadrupole insulators, Phys. Rev. Lett. **125**, 166801 (2020).

[30] Y. Qi, C. Qiu, M. Xiao, H. He, M. Ke, and Z. Liu, Acoustic realization of quadrupole topological insulators, Phys. Rev. Lett. **124**, 206601 (2020).

[31] Y.-B. Choi, Y. Xie, C.-Z. Chen, J. Park, S.-B. Song, J. Yoon, B. J. Kim, T. Taniguchi, K. Watanabe, J. Kim, K. C. Fong, M. N. Ali, K. T. Law, and G. H. Lee, Evidence of higher-order topology in multilayer WTe_2 from Josephson coupling through anisotropic hinge states, Nat. Mater. **19**, 974 (2020).

[32] C.-A. Li and S.-S. Wu, Topological states in generalized electric quadrupole insulators, Phys. Rev. B **101**, 195309 (2020).

[33] C.-A. Li, S.-B. Zhang, J. Li, and B. Trauzettel, Higher-order Fabry-Pérot interferometer from topological hinge states, Phys. Rev. Lett. **127**, 026803 (2021).

[34] Y.-B. Yang, K. Li, L.-M. Duan, and Y. Xu, Higher-order topological Anderson insulators, Phys. Rev. B **103**, 085408 (2021).

[35] Q. Wei, X. Zhang, W. Deng, J. Lu, X. Huang, M. Yan, G. Chen, Z. Liu, and S. Jia, 3D hinge transport in acoustic higher-order topological insulators, Phys. Rev. Lett. **127**, 255501 (2021).

[36] B. Liu, L. Xian, H. Mu, G. Zhao, Z. Liu, A. Rubio, and Z. F. Wang, Higher-order band topology in twisted Moiré superlattice, Phys. Rev. Lett. **126**, 066401 (2021).

[37] J. Schulz, J. Noh, W. A. Benalcazar, G. Bahl, and G. von Freymann, Photonic quadrupole topological insulator using orbital-induced synthetic flux, Nat. Commun. **13**, 6597 (2022).

[38] W. A. Benalcazar and A. Cerjan, Chiral-symmetric higher-order topological phases of matter, Phys. Rev. Lett. **128**, 127601 (2022).

[39] Z. Lei, Y. Deng, and L. Li, Topological classification of higher-order topological phases with nested band inversion surfaces, Phys. Rev. B **106**, 245105 (2022).

[40] Y. Zhou and R. Wu, Remote control of spin polarization of topological corner states, Phys. Rev. B **107**, 035412 (2023).

[41] X.-J. Luo and F. Wu, Generalization of Benalcazar-Bernevig-Hughes model to arbitrary dimensions, Phys. Rev. B **108**, 075143 (2023).

[42] W. P. Su, J. R. Schrieffer, and A. J. Heeger, Solitons in polyacetylene, Phys. Rev. Lett. **42**, 1698 (1979).

[43] F. Liu and K. Wakabayashi, Novel topological phase with a zero Berry curvature, Phys. Rev. Lett. **118**, 076803 (2017).

[44] C.-A. Li, S.-J. Choi, S.-B. Zhang, and B. Trauzettel, Dirac states in an inclined two-dimensional Su-Schrieffer-Heeger model, Phys. Rev. Res. **4**, 023193 (2022).

[45] Z. Y. Chen, S. A. Yang, and Y. X. Zhao, Brillouin Klein bottle from artificial gauge fields, Nat. Commun. **13**, 2215 (2022).

[46] C. Zhang, Z. Y. Chen, Z. Zhang, and Y. X. Zhao, General theory of momentum-space nonsymmorphic symmetry, Phys. Rev. Lett. **130**, 256601 (2023).

[47] Z. Y. Chen, Z. Zhang, S. A. Yang, and Y. X. Zhao, Classification of time-reversal-invariant crystals with gauge structures, Nat. Commun. **14**, 743 (2023).

[48] Y. X. Zhao, Y.-X. Huang, and S. A. Yang, Z_2-projective translational symmetry protected topological phases, Phys. Rev. B **102**, 161117(R) (2020).

[49] J. Hu, S. Zhuang, and Y. Yang, Synthetic gauge fields enable high-order topology on Brillouin real projective plane, arXiv:2306.15477.

[50] Y.-L. Tao, J.-H. Wang, and Y. Xu, Quadrupole insulator without corner states in the energy spectrum, arXiv:2307.00486.

[51] H. Xue, Z. Wang, Y.-X. Huang, Z. Cheng, L. Yu, Y. X. Foo, Y. X. Zhao, S. A. Yang, and B. Zhang, Projectively enriched symmetry and topology in acoustic crystals, Phys. Rev. Lett. **128**, 116802 (2022).

[52] T. Li, J. Du, Q. Zhang, Y. Li, X. Fan, F. Zhang, and C. Qiu, Acoustic Möbius insulators from projective symmetry, Phys. Rev. Lett. **128**, 116803 (2022).

[53] S. Bao, J. Chang, J. Wu, and Z. Xu, Circuit realization of Möbius insulators, Phys. Rev. A **108**, 013508 (2023).

[54] C. Jiang, Y. Song, X. Li, P. Lu, and S. Ke, Photonic Mobius topological insulator from projective symmetry in multiorbital waveguides, Opt. Lett. **48**, 2337 (2023).

[55] Y. Wang, C. Zhang, Z. Y. Chen, B. Liang, Y. X. Zhao, and J. Cheng, Chess-board acoustic crystals with momentum-space nonsymmorphic symmetries, arXiv:2305.07174.

[56] Z. Zhu, L. Yang, J. Wu, Y. Meng, X. Xi, B. Yan, J. Chen, J. Liu, X. Huang, W. Deng, C. Shang, P. P. Shum, Y. Yang, H. Chen, G. G. Liu, Z. Liu, and Z. Gao, Brillouin Klein space and half-turn space in three-dimensional acoustic crystals, arXiv:2305.08450.

[57] Y.-L. Tao, M. Yan, M. Peng, Q. Wei, Z. Cui, S. A. Yang, G. Chen, and Y. Xu, Higher-order Klein bottle topological insulator in three-dimensional acoustic crystals, arXiv:2305.09174.

[58] J. Yang and Z.-X. Liu, Irreducible projective representations and their physical applications, J. Phys. A **51**, 025207 (2018).

[59] X.-J. Luo, X.-H. Pan, C.-X. Liu, and X. Liu, Higher-order topological phases emerging from Su-Schrieffer-Heeger stacking, Phys. Rev. B **107**, 045118 (2023).

[60] C. K. Chiu, Y. H. Chan, and A. P. Schnyder, Quantized Berry phase and surface states under reflection symmetry or space-time inversion symmetry, arXiv:1810.04094.

[61] W. A. Wheeler, L. K. Wagner, and T. L. Hughes, Many-body electric multipole operators in extended systems, Phys. Rev. B **100**, 245135 (2019).

[62] B. Kang, K. Shiozaki, and G. Y. Cho, Many-body order parameters for multipoles in solids, Phys. Rev. B **100**, 245134 (2019).

[63] A. P. Schnyder, S. Ryu, A. Furusaki, and A. W. W. Ludwig, Classification of topological insulators and superconductors in three spatial dimensions, Phys. Rev. B **78**, 195125 (2008).

[64] C.-K. Chiu, J. C. Y. Teo, A. P. Schnyder, and S. Ryu, Classification of topological quantum matter with symmetries, Rev. Mod. Phys. **88**, 035005 (2016).

[65] C.-A. Li, S.-B. Zhang, J. C. Budich, and B. Trauzettel, Transition from metal to higher-order topological insulator driven by random flux, Phys. Rev. B **106**, L081410 (2022).

[66] C.-A. Li, Pseudo chiral anomaly in zigzag graphene ribbons, J. Phys.: Condens. Matter **32**, 025301 (2020).

[67] S. Ryu and Y. Hatsugai, Topological origin of zero-energy edge states in particle-hole symmetric systems, Phys. Rev. Lett. **89**, 077002 (2002).